A transfer matrix approach to conductance in quantum waveguides

1996 J. Phys.: Condens. Matter 8 3635

(http://iopscience.iop.org/0953-8984/8/20/009)

J. Phys.: Condens. Matter **8** (1996) 3635–3645. Printed in the UK

A transfer matrix approach to conductance in quantum waveguides

Wei-Dong Sheng and Jian-Bai Xia

CCAST (World Laboratory), PO Box 8730, Beijing, 100080, and National Laboratory for Superlattices and Microstructures, Institute of Semiconductors, Chinese Academy of Sciences, PO Box 912, Beijing 100083, People's Republic of China

Received 22 August 1995, in final form 2 January 1996

Abstract. A transfer matrix approach is presented for the study of electron conduction in an arbitrarily shaped cavity structure embedded in a quantum wire. Using the boundary conditions for wave functions, the transfer matrix at an interface with a discontinuous potential boundary is obtained for the first time. The total transfer matrix is calculated by multiplication of the transfer matrix for each segment of the structure as well as numerical integration of coupled second-order differential equations. The proposed method is applied to the evaluation of the conductance and the electron probability density in several typical cavity structures. The effect of the geometrical features on the electron transmission is discussed in detail. In the numerical calculations, the method is found to be more efficient than most of the other methods in the literature and the results are found to be in excellent agreement with those obtained by the recursive Green's function method.

1. Introduction

Recent advances in nanometre-scale lithography and atomic-layer epitaxy have attracted much attention to the studies of mesoscopic systems, especially after the discovery of the quantized conductance phenomenon [1, 2]. A large amount of both experimental and theoretical research on ballistic electron transport in quantum waveguides with various configurations has been reported over the past few years [3–15]. Several theoretical and numerical methods, such as the mode-matching method [4–6], the recursive Green's function method [7, 8], the transfer matrix approach [12–15] and the time-dependent approach [9, 10], have been extensively used for the investigation of electron conduction in quantum waveguides. Most of the methods have become well established, except the transfer matrix method. To the best of our knowledge, the transfer matrix at an interface with a discontinuous potential boundary has not been obtained by any authors, which limits the generality of the transfer matrix method. Only Wu *et al* [14] have developed a transfer matrix method, which can only be applied to the case of a structure with simple geometry. Xu [13] also made use of a transfer matrix method to investigate the electron wave propagation through a quantum wire with a *uniform* width under an inhomogeneous external potential. So further study of whether the transfer matrix method can be applied to investigate transport properties in complicated geometries is merited. In real electron waveguides where the boundaries are defined via electrostatic confinement from metal gates the geometries are complicated; hence, the study of realistic waveguide structure is very much necessary, though many fundamental transport properties have been found in the study of

0953-8984/96/203635+11$19.50

idealized structure. In this paper, we have proposed a transfer matrix method in which the transfer matrix at an interface with a discontinuous potential boundary is obtained. The total transfer matrix is evaluated by multiplication of the transfer matrix for each segment of the structure and by numerical integration of coupled second-order differential equations. We make use of the two methods to study several typical cavity structures and investigate the influence of the geometrical features on the electron wave propagation.

2. General formalism

We start from the two-dimensional Schrödinger equation written as

$$\left[-\frac{\hbar^2}{2m^*}\left(\frac{\partial^2}{\partial x^2}+\frac{\partial^2}{\partial y^2}\right)+V(x,y)\right]\Psi(x,y)=E\Psi(x,y) \tag{1}$$

where m^* is the electron effective mass, E is the electron energy and $\Psi(x,y)$ is the electron wave function. $V(x,y)$ represents a confining potential. Here, we assume hard-wall confinement for simplicity though it is not difficult to treat other confining potentials.

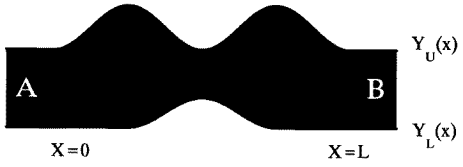

Figure 1. A plan view of the cavity structure embedded in a quantum wire. The width of the wire is W and the longitudinal length of the cavity is L.

The cavity structure is defined by $Y_L(x) < y < Y_U(x)$ and $0 < x < L$ as shown in figure 1. In the regions where $x < 0$ and $x > L$ we assume that the quantum wire is a straight line parallel to the x-axis, and the wave functions are written as

$$\begin{aligned}\Psi^A(x,y)&=\sum_{n=1}^{N}\left(a_n^A\mathrm{e}^{\mathrm{i}K_nx}+b_n^A\mathrm{e}^{-\mathrm{i}K_nx}\right)\sin\left(\frac{n\pi}{W}y\right)\\ \Psi^B(x,y)&=\sum_{n=1}^{N}\left(a_n^B\mathrm{e}^{\mathrm{i}K_nx}+b_n^B\mathrm{e}^{-\mathrm{i}K_nx}\right)\sin\left(\frac{n\pi}{W}y\right)\end{aligned} \tag{2}$$

where K_n is the longitudinal wave number and satisfies

$$\frac{\hbar^2K_n^2}{2m^*}+\frac{\hbar^2}{2m^*}\left(\frac{n\pi}{W}\right)^2=E. \tag{3}$$

The sum over n includes evanescent modes for which the wave number K_n is imaginary. N represents the number of states involved in the electron transport.

In the transfer matrix form, the coefficients a_n^A, b_n^A and a_n^B, b_n^B are related by a transfer matrix $\mathbf{M}$:

$$\begin{bmatrix}\mathbf{A}_a\\ \mathbf{A}_b\end{bmatrix}=\mathbf{M}\begin{bmatrix}\mathbf{B}_a\\ \mathbf{B}_b\end{bmatrix}=\begin{bmatrix}\mathbf{M}_1 & \mathbf{M}_3\\ \mathbf{M}_2 & \mathbf{M}_4\end{bmatrix}\begin{bmatrix}\mathbf{B}_a\\ \mathbf{B}_b\end{bmatrix} \tag{4}$$

where $\mathbf{A}_a, \mathbf{A}_b, \mathbf{B}_a$, and $\mathbf{B}_b$ are one-column matrices with elements a_n^A, b_n^A, a_n^B, and b_n^B respectively. The transfer matrix $\mathbf{M}$ is a $2N$-by-$2N$ matrix which transforms and mixes the

modes in the regions A and B [14]. If the region B is the output lead, all elements of $\mathbf{B}_b$ must vanish since it represents backward-going waves. Thus, equation (4) becomes

$$\begin{aligned} \mathbf{A}_a &= \mathbf{M}_1 \mathbf{B}_a \\ \mathbf{A}_b &= \mathbf{M}_2 \mathbf{B}_a. \end{aligned} \tag{5}$$

Once the matrices $\mathbf{M}_1$ and $\mathbf{M}_2$ are known, the transmission amplitude t and reflection amplitude r can be calculated easily. For example, supposing electrons propagate in the ground transverse mode of the quantum wire, the matrices $\mathbf{A}_a$, $\mathbf{A}_b$, and $\mathbf{B}_a$ can be written as follows:

$$\mathbf{A}_a = \begin{bmatrix} k_1^{-1/2} \\ 0 \\ \vdots \\ 0 \end{bmatrix} \qquad \mathbf{A}_b = \begin{bmatrix} r_{11}k_1^{-1/2} \\ r_{21}k_2^{-1/2} \\ \vdots \\ r_{n1}k_n^{-1/2} \end{bmatrix} \qquad \mathbf{B}_a = \begin{bmatrix} t_{11}k_1^{-1/2} \\ t_{21}k_2^{-1/2} \\ \vdots \\ t_{n1}k_n^{-1/2} \end{bmatrix}. \tag{6}$$

Since all elements of $\mathbf{A}_a$ are known, $\mathbf{B}_a$ and $\mathbf{A}_b$ can be calculated successively from $\mathbf{B}_a = \mathbf{M}_1^{-1}\mathbf{A}_a$ and $\mathbf{A}_b = \mathbf{M}_2\mathbf{B}_a$. Then the scattering amplitudes t and r can be obtained, and the conductance G can be evaluated using the two-probe Landauer–Büttiker formula [16, 17]

$$G = \frac{2e^2}{h}|t_{11}|^2. \tag{7}$$

Current conservation requires that the unitarity condition be satisfied, $|t|^2 + |r|^2 = 1$. This will serve as a check of numerical calculations. If the electron energy is larger than the second transverse energy level, then we should calculate t_{ij} and r_{ij} $(i, j = 1, 2)$. The total transmission amplitude equals $\sum_{i,j}|t_{ij}|^2$, and the total reflection amplitude equals $\sum_{i,j}|r_{ij}|^2$. The unitarity condition is

$$\sum_i \left[|t_{ij}|^2 + |r_{ij}|^2\right] = 1 \qquad \text{for } j = 1, 2.$$

In the following section, we will give two methods for calculating the total transfer matrix.

3. The transfer matrix method

At first we calculate the transfer matrix at an interface with a discontinuous potential boundary. As a check, we calculated the transmission amplitude for the well-known T-shaped structure, which has been studied by the Green's function method [8] and the mode-matching method [14]. Wu *et al* [14] solved the Schrödinger equation directly as a mode-matching problem, and gave the transfer matrix for the whole T-shaped structure. Here we give the transfer matrices for both ends of the structure, $\mathbf{M}_l$ and $\mathbf{M}_r$, and the total transfer matrix $\mathbf{M}_T$ is a product of three parts:

$$\mathbf{M}_T = \mathbf{M}_l\mathbf{M}_m\mathbf{M}_r \tag{8}$$

where $\mathbf{M}_m$ is the transfer matrix for the middle region, which is easily given.

The continuity of the wave function at a discontinuous boundary requires that

$$\sum_{n=1}^{N}(a_n^k + b_n^k)\sqrt{\frac{2}{D_k}}\sin\left(\frac{n\pi}{D_k}y\right) = \sum_{n=1}^{N}\left(a_n^{k+1} + b_n^{k+1}\right)\sqrt{\frac{2}{D_{k+1}}}\sin\left(\frac{n\pi}{D_{k+1}}y\right) \tag{9}$$

where the indices k and $k+1$ refer to the left-hand and right-hand sides of the end, and D_k and D_{k+1} are the widths of the channels. Similarly, matching the first derivatives of the wave functions at the end gives

$$\sum_{n=1}^{N} K_n^k (a_n^k - b_n^k)\sqrt{\frac{2}{D_k}}\sin\left(\frac{n\pi}{D_k}y\right) = \sum_{n=1}^{N} K_n^{k+1}\left(a_n^{k+1} - b_n^{k+1}\right)\sqrt{\frac{2}{D_{k+1}}}\sin\left(\frac{n\pi}{D_{k+1}}y\right). \tag{10}$$

K_n is the wave vector as defined in equation (3).

There are two cases: $D_{k+1} > D_k$ for the left-hand end, and $D_{k+1} < D_k$ for the right-hand end. For $D_{k+1} > D_k$ we multiply both sides of equation (9) by $\sqrt{2/D_{k+1}}\sin((m\pi/D_{k+1})y)$, integrate from zero to D_{k+1}, and obtain

$$\sum_{n=1}^{N}(a_n^k + b_n^k)S_{nm} = a_m^{k+1} + b_m^{k+1} \tag{11}$$

where

$$S_{nm} = \frac{2}{\sqrt{D_k D_{k+1}}}\int_0^{D_k}\sin\left(\frac{n\pi}{D_k}y\right)\sin\left(\frac{m\pi}{D_{k+1}}y\right)\,\mathrm{d}y \tag{12}$$

and the upper limit of the integration is taken as D_k instead of D_{k+1} because in the region $D_{k+1} > y > D_k$ the wave function of the left-hand side (denoted by k) equals zero.

We must be cautious in integrating equation (10). If we multiply both sides by $\sqrt{2/D_{k+1}}\sin((m\pi/D_{k+1})y)$, and integrate from zero to D_{k+1}, which is just the same as the way in which we treat equation (9), it implies that the derivative of the wave function in the region $D_{k+1} > y > D_k$ is also zero. This will not give a correct result and the calculated transmission amplitude always equals unity. So we should multiply both sides of equation (10) by $\sqrt{2/D_k}\sin((m\pi/D_k)y)$, integrate from zero to D_k, and obtain

$$K_m^k(a_m^k - b_m^k) = \sum_{n=1}^{N} S_{mn}K_n^{k+1}\left(a_n^{k+1} - b_n^{k+1}\right). \tag{13}$$

We can rewrite equations (11) and (13) using the matrix form equation (4) and obtain the matrix

$$\mathbf{M}_l = \frac{1}{2}\begin{bmatrix} \mathbf{M}^+ + \mathbf{M}^- & \mathbf{M}^+ - \mathbf{M}^- \\ \mathbf{M}^+ - \mathbf{M}^- & \mathbf{M}^+ + \mathbf{M}^- \end{bmatrix} \tag{14}$$

where $\mathbf{M}^+ = (\mathbf{S}^{\mathrm{T}})^{-1}$ and $\mathbf{M}^- = (\mathbf{K}^k)^{-1}\mathbf{S}\mathbf{K}^{k+1}$. $\mathbf{S}$ is the matrix with elements S_{nm} as defined by equation (12); $\mathbf{K}^k$ is the column vector with elements K_n^k. Similarly we can obtain the transfer matrix $\mathbf{M}_r$ for the right-hand end, and the total transfer matrix $\mathbf{M}_T$. Our results are completely consistent with those obtained by the mode-matching method [14].

In order to obtain the transfer matrix for a structure of arbitrary shape, we divide the plan-view pattern of the structure into segments as shown in figure 2. For each segment we obtain a transfer matrix $\mathbf{M}_k$, and the total transfer matrix is a product of all the $\mathbf{M}_k$s:

$$\mathbf{M} = \prod_k \mathbf{M}_k \tag{15}$$

where

$$\mathbf{M}_k = \frac{1}{2}\begin{bmatrix} \mathbf{M}^+ + \mathbf{M}^- & \mathbf{M}^+ - \mathbf{M}^- \\ \mathbf{M}^+ - \mathbf{M}^- & \mathbf{M}^+ + \mathbf{M}^- \end{bmatrix}\begin{bmatrix} \mathbf{P}^- & \mathbf{0} \\ \mathbf{0} & \mathbf{P}^+ \end{bmatrix} \tag{16}$$

$$(\mathbf{P}^-)_{nm} = \mathrm{e}^{-\mathrm{i}K_m^{k+1}d}\delta_{nm} \tag{17}$$

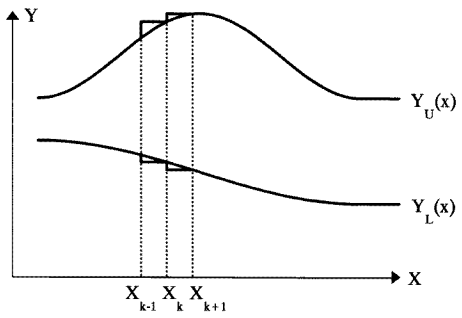

Figure 2. Coordinates of the calculation.

$$(\mathbf{P}^{+})_{nm} = \mathrm{e}^{\mathrm{i}K_m^{k+1}d}\delta_{nm}. \tag{18}$$

$\mathbf{P}^{-}$ and $\mathbf{P}^{+}$ are the transfer matrices in the segment; d is the width of the segment.

Although the slicing of the waveguide region into finite elements is not a new idea in the studies of ballistic transport in mesoscopic systems and is often used in treating disorder effects in a quantum wire with uniform width [13], we should note that this technique is seldom used to treat structure with complicated geometry. The technique is also usually used in the recursive Green's function method which is based on the tight-binding model. The slicing of a quantum wire with uniform width into finite elements would not change the boundaries of the structure while the application of the technique to a structure with complicated geometry would certainly change the boundaries. As we know that the electron transmission is dependent on the geometrical features of the waveguide, whether or not the slicing technique can be applied to the complicated geometries is a problem left unsettled. In section 5, we will check our method by comparison of the results with those obtained by the numerical method proposed in the next section and the recursive Green's function method.

4. The numerical method

Besides the method proposed in the last section, there are other methods [12, 14, 15] for evaluating the total transfer matrix method not via the definition of the transfer matrix. These methods are usually called numerical methods not transfer matrix methods. In this section, we propose a numerical method for evaluating the total transfer matrix by numerical integration of coupled second-order differential equations. The numerical method requires that the two boundary functions $Y_L(x)$ and $Y_U(x)$ be continuous, and that their first and second derivatives with respect to x exist.

In the interior cavity, the wave function takes the following form [12] for $0 < x < L$:

$$\Psi^{C}(x, y) = \sum_{n=1}^{N} f_n(x)\Phi_n(x, y) \tag{19}$$

where

$$\Phi_n(x, y) = \sin\left[\frac{n\pi}{d(x)}(y - Y_L(x))\right]$$

and $d(x) = Y_U(x) - Y_L(x)$. Insertion of the above equation into equation (1) gives

$$\sum_{n=1}^{N}\left[\Phi_n(x,y)\frac{\mathrm{d}^2 f_n(x)}{\mathrm{d}x^2} + 2\frac{\partial\Phi_n(x,y)}{\partial x}\frac{\mathrm{d}f_n(x)}{\mathrm{d}x} + \frac{\partial^2\Phi_n(x,y)}{\partial x^2}f_n(x)\right]$$
$$= \sum_{n=1}^{N}\left[\left(\frac{n\pi}{d(x)}\right)^2 - k^2\right]\Phi_n(x,y)f_n(x) \tag{20}$$

where $\overline{h}^2k^2/2m^* = E$. Multiplying the above equation by $\Phi_m^*(x,y)$ and integrating for y from $Y_L(x)$ to $Y_U(x)$, we obtain the following equation:

$$\frac{\mathrm{d}^2 f_m(x)}{\mathrm{d}x^2} = \left[\left(\frac{m\pi}{d(x)}\right)^2 - k^2\right]f_m(x) - \sum_n V_{mn}(x)f_m(x)$$
$$- \sum_n U_{mn}(x)\frac{\mathrm{d}f_m(x)}{\mathrm{d}x} \qquad m = 1, 2, \ldots, N \tag{21}$$

where

$$V_{mn}(x) = \frac{2}{d(x)}\int_{Y_L(x)}^{Y_U(x)}\Phi_m(x,y)\frac{\partial^2\Phi_n(x,y)}{\partial x^2}\,\mathrm{d}y$$
$$U_{mn}(x) = \frac{4}{d(x)}\int_{Y_L(x)}^{Y_U(x)}\Phi_m(x,y)\frac{\partial\Phi_n(x,y)}{\partial x}\,\mathrm{d}y. \tag{22}$$

Equation (21) is a system of second-order differential equations, which can be solved by a numerical method—for example, the Adams 'once prediction and twice correction' method [18, 19]. At the right-hand end of the cavity, we give the boundary condition for $\mathrm{e}^{\mathrm{i}k_n x}$; for simplicity, the origin of the coordinates can be placed at the right-hand end. Then we integrate equation (21) by the Adams method from the right-hand end to the left-hand end, and obtain the values of the wave functions $f_m(x)$ and their first derivatives $f'_m(x)$ at the left-hand end. From the definition of the transfer matrix, equation (5), we obtain the matrix elements

$$(M_1)_{mn} = \frac{1}{2}\left(f_m(0) + \frac{f'_m(0)}{\mathrm{i}k_m}\right)$$
$$(M_2)_{mn} = \frac{1}{2}\left(f_m(0) - \frac{f'_m(0)}{\mathrm{i}k_m}\right) \tag{23}$$

from the boundary condition $\mathrm{e}^{\mathrm{i}k_n x}$ at the right-hand end.

5. Results and discussion

In the above sections, we have proposed two methods; one is the transfer matrix method and the other is the numerical method. In this section, we use the two methods to investigate the electron wave propagation in several typical cavity structures and compare our results with those obtained by the recursive Green's function method. In all of our calculations, the unitarity condition is satisfied within an error of 10^{-3}.

In figure 3, we provide the results for a triangular cavity structure as shown in the inset. The triangular cavity has symmetric geometry with respect to the two terminals, and its length and height are $2W$. The results shown as a solid line were calculated by our transfer matrix method, and those shown as a dotted line were obtained by the recursive Green's function method. In the numerical calculations, we divide the cavity into 20 segments along the longitudinal direction, and the number of the transverse modes N is chosen to be 5.

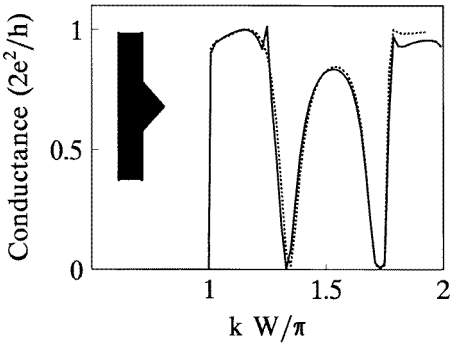

Figure 3. The conductance G in units of $2e^2/h$ versus kW/π for a triangular cavity structure calculated by our transfer matrix method (solid line) and the recursive Green's function method (dotted line). A schematic view of the structure is shown in the inset of this figure.

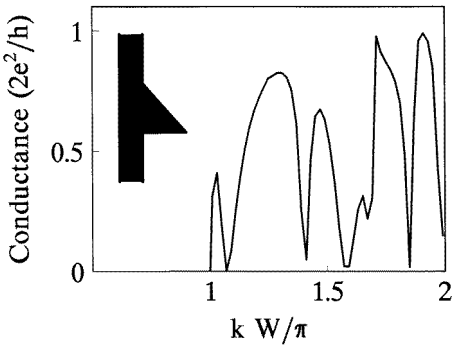

Figure 4. For another triangular cavity structure, the conductance G in units of $2e^2/h$ versus kW/π calculated by our transfer matrix method. A schematic view of the structure is shown in the inset of this figure.

In the recursive Green's function method, we construct a two-dimensional mesh with a lattice constant $a = 0.05W$ [8], and the maximum dimension of the matrices involved in the computation is 40, while it is only 10 in our method. In the actual computation, we find that our transfer matrix method is more efficient than the recursive Green's function method, while the results obtained by the two methods are found to be in excellent agreement with each other. As we have seen from figure 3, we obtain the desired results by slicing the cavity into only 20 segments, i.e., the electron transmission is not very sensitive to geometrical features of the structure. Therefore, the effectiveness of the slicing technique is verified in treating the electron wave propagation in complicated geometries. In figure 4, we provide the results for another triangular cavity structure with a discontinuous potential boundary. As the function $Y_U(x)$ for the upper boundary is not continuous, our numerical method cannot be applied. For the structure with a discontinuous potential boundary, there are many resonant peaks in the transmission profile due to the enhanced mode-mixing effect [12].

Using our numerical method, we have studied the electron wave propagation in four typical cavity structures. In the numerical calculations, we set $N = 5$ and find it sufficient for obtaining the desired results [12]. We provide the results for a symmetric double-stub structure in figure 5(a) in which the solid line is for the cavity of maximum width $2W$ and the dotted line is for the cavity of maximum width $3W$. Compared with the structure shown in figure 3, the cavity considered here is not small, while we find that the transmission profiles are simpler than that in figure 3. This phenomenon would be explained if the transverse modes involved in the transport in the cavity are much reduced due to the symmetry of the cavity. As the structure has symmetry with respect to the central line of the quantum wire, the transverse states in the structure can be classified into two types: one for those with even symmetry, the other for those with odd symmetry. If the incident electron transports in the fundamental transverse mode in the terminal, the electron wave function has even symmetry, and we need not take those transverse modes with odd symmetry in the cavity into account because they do not contribute to the wave propagation. As the number of transverse modes involved in transport in the cavity is reduced, the interference effect is not so obvious as that in the structure shown in figure 3, and the transmission profile exhibits

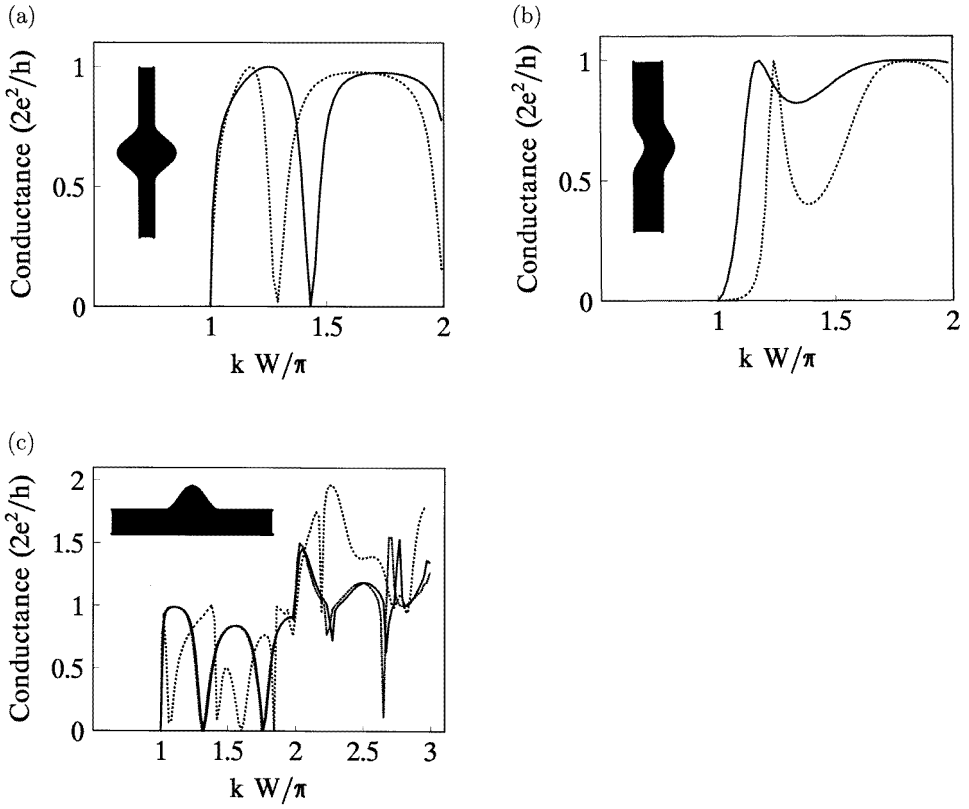

Figure 5. (a) For a symmetric cavity structure with $L = 2W$, and $D(x) = W\{1 + b[1 + \cos(2x/L - 1)\pi)]\}$, the conductance G in units of $2e^2/h$ versus kW/π calculated by our numerical method; the solid line is for $b = 1$ and the dotted line is for $b = 1.5$. A schematic view of the structure is shown in the inset of this figure. (b) For a cavity structure with $L = 2W$, $D(x) = W$ and $Y_L(x) = bW[1 + \cos(2x/L - 1)\pi)]$, the conductance G in units of $2e^2/h$ versus kW/π calculated by our numerical method; the solid line is for $b = 0.2$ and the dotted line is for $b = 0.3$. A schematic view of the structure is shown in the inset of this figure. (c) For a cavity structure with $L = 2W$, $Y_L(x) = 0$ and $D(x) = W\{1+b[1+\cos(2x/L-1)\pi)]\}$, the conductance G in units of $2e^2/h$ versus kW/π calculated by our numerical method (the solid line is for $b = 0.5$, and the dotted line is for $b = 1$) and our transfer matrix method (the chain line is for $b = 0.5$). A schematic view of the structure is shown in the inset of this figure.

simple structure.

In figure 5(b), we provide the results for a structure with wide–narrow–wide geometry. Although the cavity width along the transverse direction is set to be the same as that of the terminal, the actual width of the cavity is smaller than that of the lead. From the figure, we can see typical transmission profiles for wide–narrow–wide geometry. In figure 5(c), we provide the results for a structure with a sinuous cavity as shown in the inset. In the figure, the solid line corresponds to the results for a cavity of maximum width $2W$ and the dotted line to those for a larger cavity of maximum width $3W$. Although the geometry of the cavity structure considered here is not similar to the well-known T-shaped structure, we find that there are many similarities between their transmission profiles [14], and we may conclude that the shape dependence of the electron transmission is relatively weak. In the

same figure, we also show the results (chain line) calculated by our transfer matrix method for comparison. We find that the results obtained by the two different methods are in good agreement with each other.

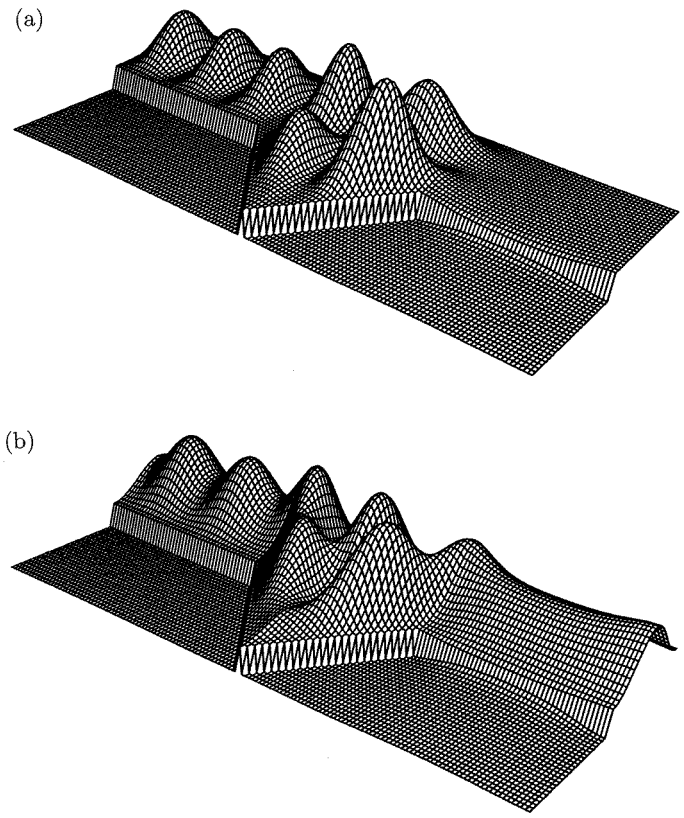

Figure 6. (a) A three-dimensional plot of the electron probability density ($|\Psi|^2$) in the triangular cavity structure for $kW/\pi = 1.73,\ T = 0.04$. (b) A three-dimensional plot of the electron probability density ($|\Psi|^2$) in the triangular cavity structure for $kW/\pi = 1.57,\ T = 0.972$.

In figures 6(a) and 6(b), we provide the three-dimensional plots of the electron probability density ($|\Psi|^2$) in the triangular cavity structure for which the transmission profile has been shown in figure 3. In the two figures, the electron is incident from the upper left. They enable us to have further insight into the electron conduction. If the electron probability density is known, the influence of other effects on the electron transmission would be readily determined without further numerical calculation. For example, we want to know how a δ-function impurity located in the cavity affects the electron wave propagation. As we know that only in the region beside the impurity is the electron probability density much changed, an impurity located at the site where the electron probability density reaches its minimum would not affect the electron transmission much. If there is an impurity located at one end of the cavity, it is almost certain that the electron transmission would be much reduced, because there is not enough space for an electron to bypass the impurity. As can be seen from the figures, the electron wave function would not penetrate into the upper corner of the cavity due to the limitation of the energy of the incident electron, which is

believed to be the main reason for which the electron wave propagation does not depend much on the geometrical features of the structure. Actually, if the incident electron is of very high energy, it is certain that the electron transmission is strongly dependent on the geometrical features. Finally, we should note that the modes in the input lead and output lead of the structure are different, because there is a reflected wave in the input lead while there is only the outgoing wave in the output lead. As there is a phase difference of π between the incoming wave and the reflected wave in the input lead, the electron probability density is very different due to the interference of the two waves in the input lead. In figure 6(a), the interference is obvious, because the incident wave is almost totally reflected. In figure 6(b), we have the transmission coefficient $T = 0.972$ and the reflection amplitude $r = \sqrt{1-T} = 0.167$. Therefore the ratio of the maximum of the electron probability density in the input lead to the minimum, $(1+r)^2/(1-r)^2$, is 1.96. So, the interference effect in the input lead is also notable even when the transmission coefficient is almost equal to 1.

In fact, the two-dimensional waveguide problem is a quantum mechanics boundary value problem, but the boundary values at the two leads should be determined simultaneously with the solution inside the cavity. This presents some difficulty, and several numerical methods have been developed as mentioned in the introduction. Our method solves the problem in real space, and obtains the transmission amplitude t and reflection amplitude r along with the wave function inside the cavity. So it provides a clear physical picture for the electron transport and offers the possibility of taking other effects into account further—such as those of impurities and confining potential profiles. For a cavity of complicated shape, our method does not require construction of a two-dimensional mesh, which is time-consuming. Besides this, our method is based on the free-electron energy band model, without the limitation of the tight-binding model used in the recursive Green's function method.

6. Conclusions

We have presented a transfer matrix approach for the study of electron conduction in an arbitrarily shaped cavity structure embedded in a quantum wire. Using the boundary conditions for wave functions, we have obtained the transfer matrix at an interface with a discontinuous potential boundary. The total transfer matrix is calculated by multiplication of the transfer matrix for each segment of the structure as well as numerical integration of coupled second-order differential equations. We have applied the proposed method to the evaluation of the conductance and the electron probability density in several typical cavity structures. We have studied the effect of the geometrical features on the electron transmission in detail and found that it is not obvious. In the numerical calculations, we have found that our transfer matrix method is more efficient than other methods in the literature. We have also found that the results are in excellent agreement with those obtained by the recursive Green's function method.

Acknowledgment

This work was supported by the Chinese National Science Foundation.

References

[1] Wharam D A, Pepper M, Ahmed H, Frost J E F, Hasko D G, Peacock D C, Ritchie D A and Jones G A C 1988 *J. Phys. C: Solid State Phys.* **21** L209

[2] van Wees B J, van Houten H, Beenakker C W J, Williamson J G, Kouwenhoven L P, Van der Marel D and Foxon C T 1988 *Phys. Rev. Lett.* **60** 848
[3] Peeters F M 1990 *Science and Engineering of One and Zero Dimensional Semiconductors* ed S P Beaumont and C M Sotomayor-Torres (New York: Plenum) p 107
[4] Takagaki Y and Ferry D K 1992 *Phys. Rev.* B **45** 6715
[5] Takagaki Y and Ferry D K 1992 *Phys. Rev.* B **45** 8506, 12 153
[6] Xia J B 1992 *Phys. Rev.* B **45** 3593
[7] Baranger H U, DiVincenzo D P, Jalabert R A and Stone A D 1991 *Phys. Rev.* B **44** 10 637
[8] Sols F, Macucci M, Ravaioli U and Hess K 1989 *J. Appl. Phys.* **66** 3892
[9] Stratford K and Beeby J L 1993 *J. Phys. C: Solid State Phys.* **5** L289
[10] Stratford K and Beeby J L 1993 *Negative Differential Resistance and Instabilities in 2-D Semiconductors* ed B K Ridley, N Balkan and A J Vickers (New York: Plenum) p 385
[11] Laughton M J, Barker J R, Nixon J A and Davies J H 1990 *Phys. Rev.* B **44** 1150
[12] Nakazato K and Blaikie R J 1991 *J. Phys. C: Solid State Phys.* **3** 5729
[13] Xu H 1993 *Phys. Rev.* B **47** 9537
[14] Wu H, Sprung D W L, Martorell J and Klarsfeld S 1991 *Phys. Rev.* B **44** 6351
[15] Wu H, Sprung D W L and Martorell J 1992 *Phys. Rev.* B **45** 11 960
[16] Landauer R 1957 *IBM J. Res. Dev.* **1** 223
[17] Büttiker M 1987 *Phys. Rev.* B **35** 4123; 1988 *Phys. Rev.* B **38** 12 724
[18] Xia J B 1988 *Phys. Rev.* B **38** 8365
[19] Lambert J D (ed) 1972 *Computational Methods in Ordinary Differential Equations* (Chichester: Wiley) p 106